Original Article

Optical coherence tomography-based deep learning algorithm for quantification of the location of the intraocular lens

Chen Xin[1#], Gui-Bin Bian[2#], Haojie Zhang[3], Weipeng Liu[3], Zhe Dong[4]

[1]Beijing Institution of Ophthalmology, Beijing Tongren Hospital, Capital Medical University, Beijing, China; [2]State Key Laboratory of Management and Control for Complex Systems, Institute of Automation, Chinese Academy of Sciences, Beijing, China; [3]College of Artificial Intelligence and Data Science, Hebei University of Technology, Tianjin, China; [4]Beijing Tongren Eye Center, Beijing Key Laboratory of Ophthalmology and Visual Science, Beijing Tongren Hospital, Capital Medical University, Beijing, China

Contributions: (I) Conception and design: Z Dong; (II) Administrative support: GB Bian; (III) Provision of study materials or patients: Z Dong; (IV) Collection and assembly of data: C Xin; (V) Data analysis and interpretation: C Xin, H Zhang, W Liu; (VI) Manuscript writing: All authors; (VII) Final approval of manuscript: All authors.

[#]These authors contributed equally to this work.

Correspondence to: Zhe Dong. Ophthalmology Department, Beijing Tongren Hospital, Capital Medical University, Dong Jiao Min Xiang 1#, Dongcheng District, Beijing, China. Email: dongzhe0@126.com.

Background: Cataract surgery has been recently developed from sight rehabilitating surgery to accurate refractive surgery. The precise concentration of intraocular lens (IOL) is crucial for postoperative high visual quanlity. The three-dimentional (3D) images of ocular anterior segment captured by optial coherence tomography (OCT) make it possible to evaluate the IOL position in 3D space, which provide insights into factors relavant to the visual quanlity and better design of new functional IOL. The deep learning algorithm potentially quantify the IOL position in an objective and efficient way.

Methods: The region-based fully convolutional network (R-FCN) was used to recogonize and delineate the IOL configuration in 3D OCT images. Scleral spur was identified automatically. Then the tilt angle of the IOL relative to the scleral spur plane along with its decentration with respect to the pupil were calculated. Repeatability and reliability of the method was evaluated by the intraclass correlation coefficient.

Results: After improvement, the R-FCN network recognition efficiency of IOL configuration reached 0.910. The ICC of reliability and repeatability of the method is 0.867 and 0.901. The average tilt angle of the IOL relative to scleral spur is located in 1.65±1.00 degrees. The offsets dx and dy occurring in the early X and Y directions of the IOL are 0.29±0.22 and 0.33±0.24 mm, respectively. The IOL offset distance is 0.44±0.33 mm.

Conclusions: We proposed a practical method to quantify the IOL postion in 3D space based on OCT images and assisted by an algorithm.

Keywords: Intraocular lens; optical coherence tomography; deep learning; position

Submitted May 01, 2020. Accepted for publication Jul 09, 2020.
doi: 10.21037/atm-20-4706
View this article at: http://dx.doi.org/10.21037/atm-20-4706

Introduction

Cataract is the leading cause of reservable blindness in the word. It is estimated that the prevalence of cataract is about 80% in the Chinese population for individuals ranging from 60 to 89 years old, with the prevalence rising to 90% in the over 90-year-old age bracket. Fortunately, this vision impairment can be reserved by a surgical procedure which combines cataract extraction and intraocular lens (IOL) implantation. A recent report showed that there are nearly 8 million cataract patients in China; however only 3,000–4,000 cases per million population received surgical

procedures. With the development of surgical equipment and people's dependence on high visual quality, cataract surgery has been developed from sight rehabilitating surgery to accurate refractive surgery. Minimally invasive technique and functional IOL are the two important directions of cataract surgery. The accurate position of the IOL is the prerequisite for the high visual quality. Recently, a variety of methods have been developed to quantitate the position of IOL, such as photography of slit lamp, scheimpflug video photography, and optical coherence tomography (OCT) (1-5).

Anterior segment OCT (AS-OCT) is especially designed for imaging of the anterior segment tissue, offering good resolution and penetration. Multiple scanning protocols provide the possibility acquire a robust contour of the IOL and further quantitate the position of IOL in a three-dimensional (3D) manner. Previous reports have presented the feasibility of quantifying the tilt and decentration of IOL—two important parameters that induce astigmatism (6-8). One study also showed that having more than 5 degrees induced by IOL could lead to relevant myopic shift and oblique astigmatism. However, in most of these studies, the identification of the anatomic landmarks was done manually by the investigator, which is tedious and time-consuming and does not allow for the quantification of a large amount of cases as the position of the IOL is quantified two dimentionally.

As the rapid development of deep learning and modern artificial intelligence technology, its practice and application in different fields have been gradually developed. The medical field is no exception. The diagnosis of ocular diseases depends on a large amount of images and doctor's clinical experience. The application of artificial intelligence technology in ophthalmology through machine learning combined with computer greatly improves the diagnostic efficiency of ocular diseases in clinical work and lightens the burden of ophthalmologists. The application of artificial intelligence in ophthalmology is still in its infancy, mainly involving most common ocular diseases such as diabetic retinopathy, glaucoma and cataract. These methods include artificial intelligence-assisted screening and diagnosis of the ocular disease, the segmentation of OCT retinal images, and others. In terms of the importance of precise IOL position and OCT priority in 3D manner and high resolution, some algorithms were presented to automatically outline the IOL in 3D way. Gillner M *et al*. recently achieved to automatically segment and detect the IOL on OCT images. Although potentially transfer to clinical application, the method based on the optomechanical eye model or porcine eyes still different from patients in clinic (9). In this study we attempted to automatically identify the configuration of the IOL and quantify the IOL bias based on 3D OCT images. A technique that can effectively quantitate the IOL for the evaluation of the lens before the cataract surgery can provide the baseline parameters for a personalized IOL in the near future. We present the following article in accordance with the MDAR reporting checklist (available at http://dx.doi.org/10.21037/atm-20-4706).

Methods

Data acquisition and preparation

This study followed the declaration of Helsinki (as revised in 2013) and was approved by the Ethics Committee of the Beijing Tongren Hospital (TRECKY2018-066). AS-OCT images from a total of 86 eyes were continuously acquired by the same operator from June 2018 to December 2019 at Beijing Tongren Eye Center. All the subjects were asked to sign the informed consent. All eyes received cataract surgery without any intra- and post-operative complication at least one year prior the recruition of the study. There is no record of any ocular disease and tramatic history for all the subjects. For each subject, the 3D structural scans of IOL were conducted by a commercially swept source OCT (Casia SS-OCT, Tomy Corporation, Nagoya, Japan) before any contact procedure, under dark room conditions. The system had a center wavelength of 1,310 nm. The subjects were asked to focus on the internal fixation target and a 3D posterior chamber scan was captured using the auto alignment function. This algorithm can take 128 consecutive meridional scans, comprising 512 A-scans across the chamber.

The AS-OCT image can clearly display the IOL contour of the anterior segment of the eye, providing a more reliable basis for diagnosing IOL eccentricity and tilt. This method has great advantages in the diagnosis of anterior tumors, cataracts, glaucoma, and other diseases and facilitating refractive surgery follow-up. The AS-OCT is specifically designed for anterior segment imaging, with good resolution and penetrating power. Various scanning protocols enable the possibility to obtain a solid outline of the IOL and further quantify the position of the IOL in

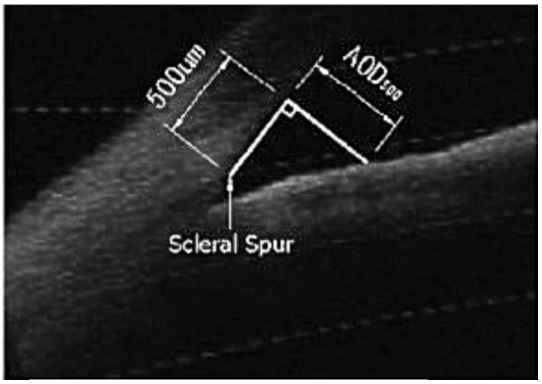

Figure 1 The scleral spur in OCT image (14). OCT, optical coherence tomography.

3D. Therefore, we used AS-OCT images to analyze IOL eccentricity and tilt.

Network architecture

Loss function (10)

Since the IOL occupies a large area in the AS-OCT impact, our goal was to locate and identify the IOL. We chose the end-to-end region-based fully convolutional network (R-FCN) network. We did not choose to modify it in the loss function (10), and it remained as follows:

$$L(s, t_x, y, w, h) = L_{cls}(s_c^*) + \lambda[c^* > 0]L_{reg}(t, t^*) \quad [1]$$

Training (10)

Training region-based object detectors with online hard example mining (OHEM) (11) were acquired through training. For example, the part in the region of interest (ROI), which has no cost in the calculation, was ignored. Assuming that each OCT image was divided into N regions, we directly calculated all losses for the N regions. By tidying up all ROI losses, we found that the percentage of losses in selected B was the highest. Backpropagation (12) was performed in the selected instance.

We set the weight decay to 0.0005 and the momentum to 0.9. By default, the training mode is unipolar training, and the short side of the image is adjusted to 600 pixels (11,13). In training, we chose to use a model of 8 Graphic processing units (GPUs). Each GPU guarantees 1 image and that B =128 ROI for backpropagation. In the training process of regional candidates network and R-FCN, we alternately train them (14). In order to enable the network's recognition and classification of IOLs to meet the needs of doctors, we replaced the classifier of the neural network. It was replaced by a random forest classifier, and the data of RPN and regularization orthogonal least squares were transmitted to the random forest classifier respectively. The two data points were scored separately and compared. The result with the highest score was selected for output.

After improvements, we trained the dataset. After considerable training, the R-FCN network's recognition rate for IOL was stabilized t above 0.910. The results show that the improved R-FCN had a higher recognition rate for IOL, which significantly improved the model's detection accuracy and feature extraction capabilities, and thus enhanced the classification ability of the model.

Imaging processing

Firstly, the location and type of IOL were identified by through edge detection of IOL using R-FCN. Then, the IOL tilt angle and optic axis angle were calculated on the relative location between IOL and scleral spur in OCT images.

Scleral spur

Scleral spur, a narrow stenosis composed of circularly oriented collagen bundles, protrudes into the anterior chamber. It is an important and constant landmark usually used to determine the opening of the anterior angle, which previously needed to be identified manually. In OCT images, scleral spur is the location where the corneal curvature changes dramatically (*Figure 1*). The plane of the scleral spur is relatively parallel to the section of the corneal apex of the human eye. Thus, the plane of the scleral spur is a good benchmark for determining the IOL tilt. Canny algorithm was used to identify the scleral spur. After removal of the signal noise in the preprocessing procedure, the image was enhanced to highlight the posterior surface of the sclera. We then connected the scleral spur on each side with a line. The recognition effect of the algorithm is shown in *Figure 2*.

Then, 12 OCT images (relatively clear images of the sclera spur) were used to evaluate the consistency of the identification of scleral spur between the doctor and the algorithm. *Figure 3* is one example of the comparison.

However, in some AS-OCT images, problems such as scanning might have made it difficult for our method to identify the sclera spur. Therefore, our method still has certain limitations.

Inclination angle of IOL in a 0-degree image

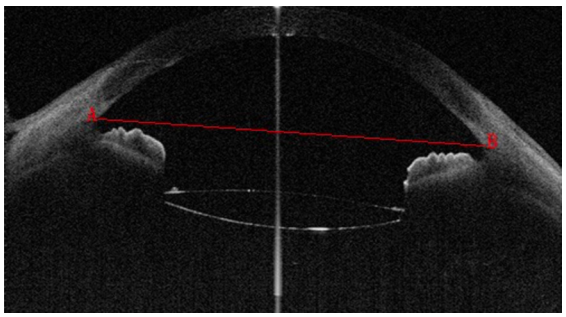

Figure 2 The linear connection between scleral spurs built up by the algorithm.

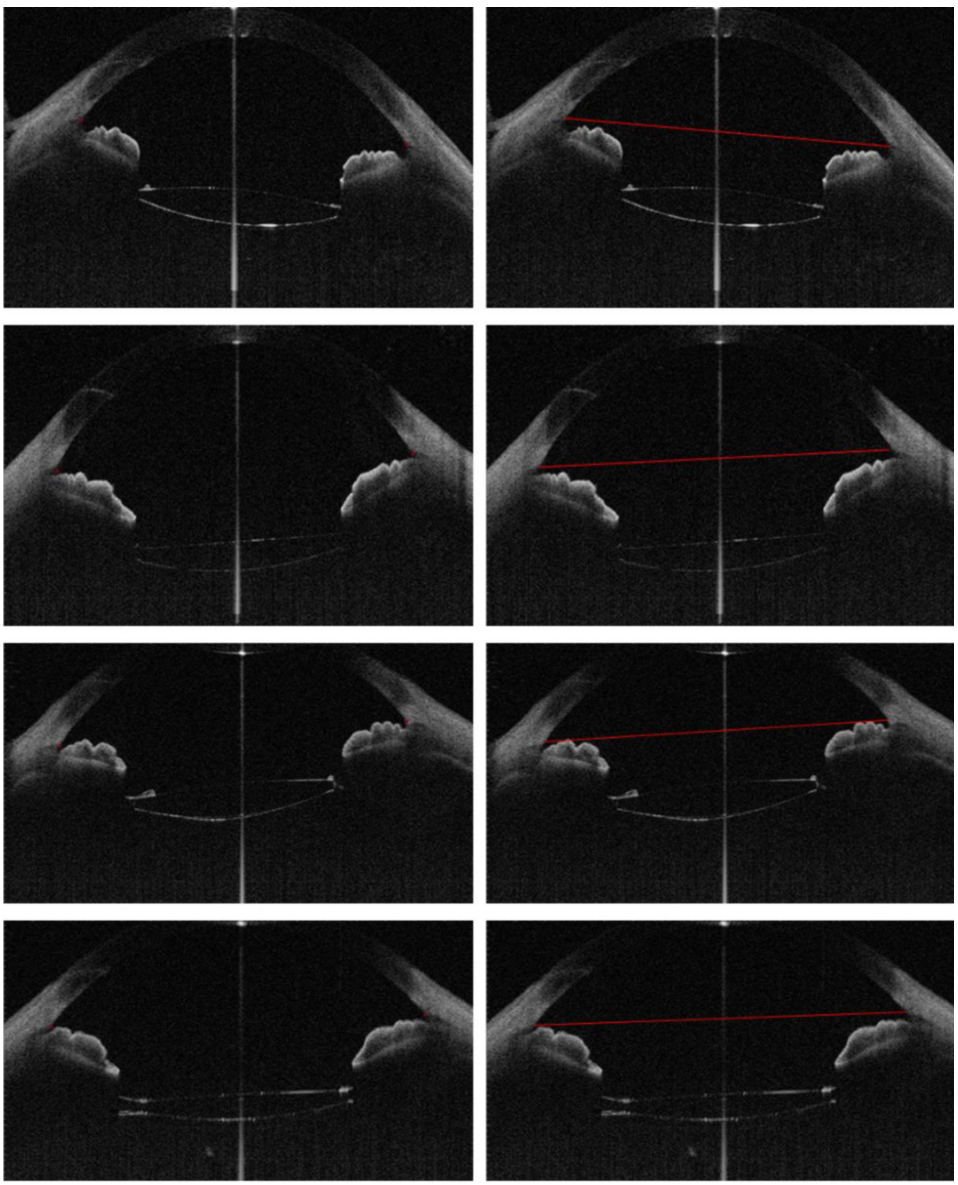

Figure 3 Scleral spur identified by a doctor (left) and the algorithm (right).

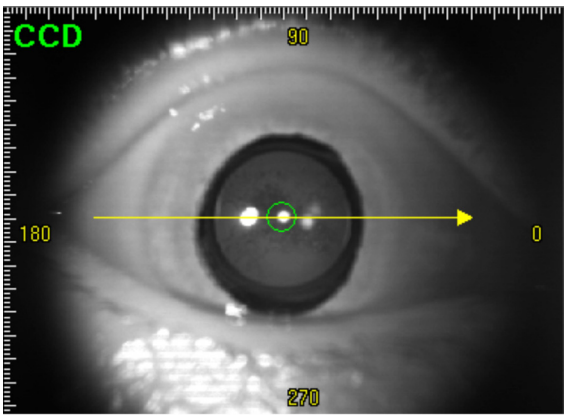

Figure 4 Plane view of ocular surface relative to the OCT scanning lens. OCT, optical coherence tomography.

In clinic, the diopter of IOL is the only parameter that can be chosen individually depending on corneal curvature, axial length, and a constant (K-value). Although the volume of the lens with cataract probably varies from person to person, the diameter of the IOL is designed uniformly by the manufacturer. The universal diameter of the IOL placed in the variable size of the capsule could induce the shifting of IOLs. On the other hand, the pupil was dilated before the surgery, and the center of the dilated pupil changes relative to its original site in its natural status. Therefore, even if the IOL is placed in the center of the pupil during the operation, it might not be centered when the pupil is constricted in daily life (*Figure 4*).

In the OCT image, the IOL tilt angle was defined as the angle between the plane of the IOL and the optic axis on the 0-degree image, which could induce aberration of the vision. The IOL tilt angle was measured as follows. The location of IOL was identified by R-FCN after selecting a 0-degree image. In the OCT image, a part of the IOL failed to appear because of the shadowing of the iris. For the regions with a clear margin of the IOL, edge detection was performed by the temporal Canny algorithm. Canny algorithm can also be used to extract IOL boundary image coordinates in the R-FCN recognition area. The boundary of IOL is fitted by binarization according to the image coordinates. As designed by the manufacture, both the anterior and posterior surfaces of the IOL are circular. Thus, according to the delineated boundary of the IOL, the diameter of both the anterior and posterior surface could be calculated. Based on this, we could supplement the missing part of the IOL in the OCT image, and the intact boundary of IOL could be obtained by supplementing. The coordinates of scleral spur were obtained directly in the OCT image (*Figure 3*). Then, the anterior and the posterior plane equations of IOL in 3D space were fitted, which is described later in detail (migration of IOL in 3D space). The examples of image processing results are shown in *Figure 5*. From the image coordinate system (*Figure 5*), we determined that the equation of the scleral spur connection was the following 10x+427y=71699. The equation of connection between two ends of the crystal was the following: x+25y=5188. Therefore, the inclination angle of the biconvex IOL was 2.86 degrees. In similar fashion, we calculated that the tilt angle of the planar IOL was 1.43 degrees (*Figure 5*).

Migration of IOL in 3D space

The inclination angle mentioned in section B is based on the 2D image of OCT, which presents limited information of the IOL in the anterior segment of whole eye. Thus, we tried to obtain the anterior and posterior plane equations of IOL in 3D space. The computational procedures to measure the tilt and decentration of IOL in the OCT images are described below (*Figure 6*).

(I) Computing the scaling ratio of the planar graph and a screenshot. The scaling factor λc on the cross section is calculated from the actual distance, with the image distance shown in *Figure 7*.

$$\lambda_c = 6.91/(x_{a_1} - x_{a_2}) \quad [2]$$

Through the corresponding relation of the point a_1 to a_1' and a_2 to a_2' in the cross-section image and plane graph, the zoom factor λp of the plane graph can be calculated as follows:

$$\lambda_p = 6.91/(x_{a_1}' - {}'x_{a_2}'') \quad [3]$$

(II) The spherical coordinates and radius of the spherical surface of IOL were obtained. Here we selected the coordinates of four different points on the anterior/posterior surfaces. The spherical coordinates and radius of the spherical surface on which the front and back surfaces of the IOL were located could be determined by several points.

In *Figure 7*, a_1, a_2, and a', a_2' are the vertices of the left and right irises in the plan graph and the screenshot respectively. B is the reference point selected in the screenshot. It is the intersection of the vertical line and the

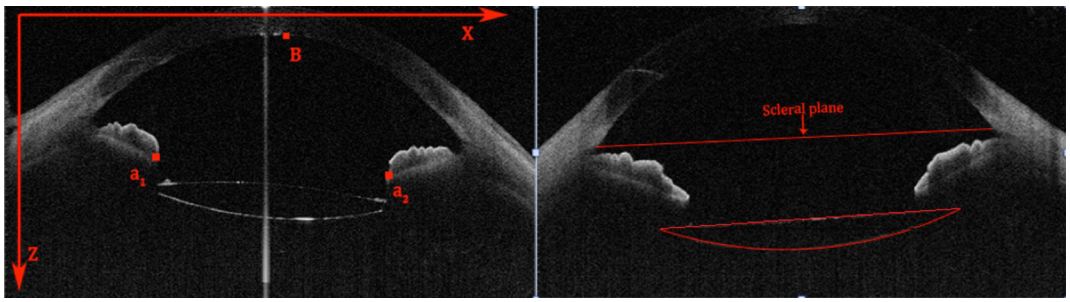

Figure 5 An example of an image processing result for the edge detection and margin supplement of IOL and the plane of the scleral spur. Left: biconvex IOL; right: planar IOL. IOL, intraocular len.

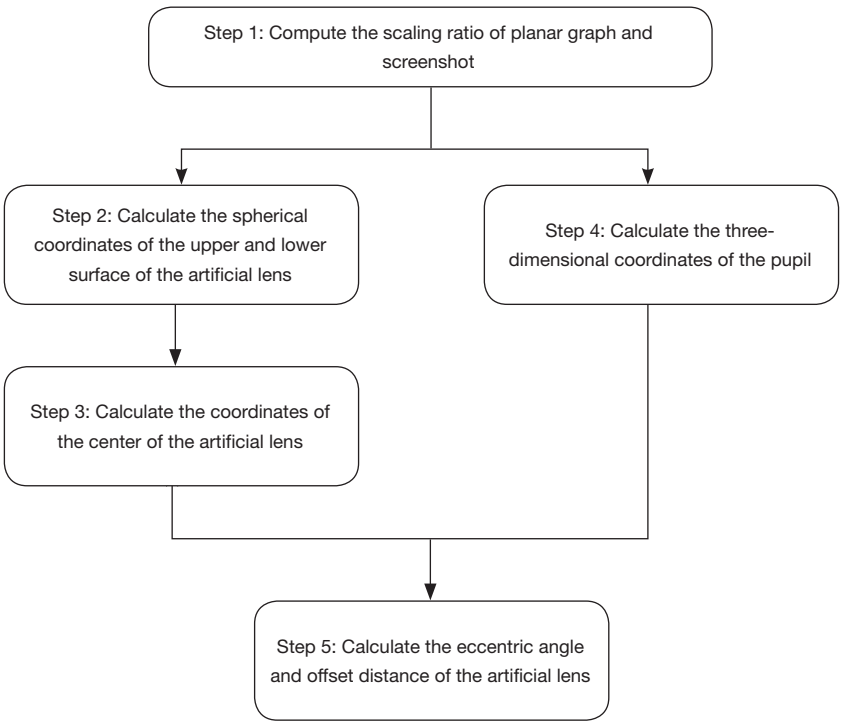

Figure 6 Flowchart for measuring IOL decentration and tilt. IOL, intraocular len.

cornea in a_1 and a_2. The pupil is defined as the midpoint of and a_1', a_2'.

After obtaining the coordinates of these points, a reference point was selected. It is point B on the cross-sectional view in *Figure 7*. Point B is the intersection of the perpendicular line with the cornea in the line connecting a_1 and a_2 in the cross section. In the plane view, point B and the midpoint of a_1 and a_2 overlap. This way, we could determine that reference point B had the following coordinates in the plan view:

(x', y') [4]

Next, by referring to the actual distances between point B and a_1 in the plan view, the x-coordinate of the point B in the section plane could be obtained using the scale factor of the section plane. Then, δ and ϵ were taken simultaneously to the minimum value as follows:

$x_B=(x' - x'_a)\lambda p / \lambda c + x'_a$ [5]

The reference point B is the pupil in the plan view. From the plan view, we understood that the Z coordinate of B coincided with a'_1. Therefore, the spatial coordinates of reference point B were the following: (x_B, y'_B, Z) [6]

We then chose to take four points on the anterior/

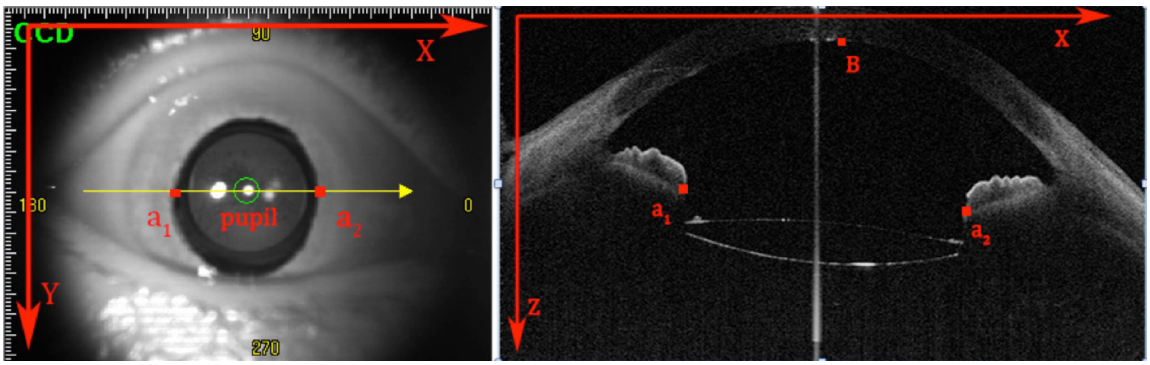

Figure 7 The diagrammatic presentation of different point symbols (the first one is a plan graph, and the second one is a 0–180 degree screenshot).

posterior surface of the IOL on the images at 0–180 degrees and 90–270 degrees, respectively. Through the coordinates of these selected points, we could determine the center and radius of the sphere where the anterior and posterior surfaces were located.

$$(x_D, y_D, z_D) = ((x^D - x^B)\lambda p, (y^D - y^B)\lambda P, (Z_D - Z_B)\lambda_C) \quad [7]$$

(III) The coordinates of the center of the IOL was calculated. Firstly, the IOL was designed as a double-convex structure. Then, the distance between the two spherical surface was determined as follows:

$$d=\sqrt{\left(x_{q1}-x_{q2}\right)^2+\left(y_{q1}-y_{q2}\right)^2+\left(z_{q1}-z_{q2}\right)^2} \quad [8]$$

The distance from the center of the sphere q1 to the center of the IOL was calculated as follows:

$$d_1=\left(R_2^1-R_2^2+d^2\right)/2d \quad [9]$$

Then, the coordinates of the center E(X_e, Y_e, Z_e) of the IOL were as follows:

$$X_e = x_{q1} + (x_{q2} - x_{q1})d_1/d \quad [10]$$

$$Y_e = y_{q1} + (y_{q2} - y_{q1})d_1/d \quad [11]$$

$$Z_e = z_{q1} + (z_{q2} - z_{q1})d_1/d \quad [12]$$

(IV) By calculating the 3D coordinates of the pupil from the geometric point of view, we determined that the 3D coordinates (X_t, Y_t, Z_t) of the pupil were the following:

$$X_t = \frac{(x_{a1} + x_{a2})\lambda_c}{2} \quad [13]$$

$$Y_t = x^B \quad [14]$$

$$Z_t = \frac{(z_{a1} + z_{a2})\lambda_c}{2} \quad [15]$$

(V) By calculating the eccentric angle and offset distance of the IOL, we determined that the center coordinates of the IOL were (X_e, Y_e, Z_e), and that the 3D coordinates of the pupil were (X_t, Y_t, Z_t). Therefore, the offset distance of the IOL was as follows:

$$\Delta x = x_e - x_t \quad [16]$$

$$\Delta y = y_e - y_t \quad [17]$$

$$\Delta z = z_e - z_t \quad [18]$$

Therefore, the eccentric distance of IOL was as follows:

$$d_s = (\Delta x)^2 + (\Delta y)^2 \quad [19]$$

The equation for the ball on the upper surface of the IOL was as follows:

$$(x - x_{q2})^2 + (y - y_{q2})^2 + (z - z_{q2})^2 = R^2 \quad [20]$$

Then, the normal equation of the upper surface of the artificial lens was as follows:

$$\frac{x-x_{q2}}{x_e-x_{q2}}=\frac{y-y_{q2}}{Y_e-y_{q2}}=\frac{z-z_{q2}}{z_e-z_{q2}} \quad [21]$$

The reference plane is the plane in which the scleral spur is located. The plane of the scleral spur is shown by the straight line in *Figure 5*. The coordinates of the scleral spur can be obtained from the OCT instrument. Therefore, the inclination angle of the IOL is the inclination angle of the normal line obtained by Equation 20 with respect to the plane. The normal of the 3D space can be obtained by the surface equation, which deviates from 1.752 degrees in the X direction, 1.445 degrees in the Y direction, and 2.860

degrees in the Z direction.

Statistical analysis

All statistical analysis was done using SPSS 23.0 (IBM, New York, NY, USA). The intraclass correlation coefficient (ICC) was used to evaluate the reliability and repeatability of the method.

Results

Repeatability and reliability

Twelve subjects were randomly chosen. The offset distance and the tilted angle of the IOL were measured for three times (*Table 1*). The first and the second measurement were done by HJZ and WPL respectively. While the third measurement was done by WPL repeatedly one month after the second measurement. The comparison of the first and second measurement were treated as reliability, the ICC of which is 0.867. The comparison of the second and the third measurement both done by WPL was defiend as repeatablility, the ICC of which is 0.901.

Table 1 Distance of IOL relative to the pupil and tilt angle of different measurements

Category	Mean ± SD (n=12)		
	Measurement 1	Measurement 2	Measurement 3
X direction offset distance	0.29±0.22 mm	0.25±0.16 mm	0.26±0.18 mm
Y direction offset distance	0.33±0.24 mm	0.29±0.22 mm	0.31±0.19 mm
Tilt angle	1.65±1.00 degrees	1.76±0.99 degrees	1.53±1.01 degrees

IOL, intraocular len.

Tilt angle and decentration of IOL in 3D space

In this study, AS-OCT images of 86 eyes were continuously acquired. Eight eyes were excluded because of the poor quality of the image. Finally 80 eyes of 58 subjects (62.3±8.6 years) in total were captured, including 32 male and 26 female. All eyes received cataract surgery at least one year prior the study. Identification and differentiation were performed by the R-FCN network IOL, and the 3D reconstruction modeling of the IOL was performed to evaluate the location of IOL. The average thickness of the IOL used in these patients was 1.30±0.24 mm. The average tilt angle of the IOL relative to the plane where the scleral spur is located in 1.65±1.00 degrees (*Figure 8*). Only one patient had a significant tilt of the IOL more than 7 degrees. It significantly affected the vision. The offsets dx and dy occurring in the early X and Y directions of the IOL are 0.29±0.22 and 0.33±0.24 mm, respectively. The IOL offset distance is 0.44±0.33 mm. As shown in *Table 2*.

Discussion

The biggest advantage of AS-OCT with respect to prior technique is the ability to provide high resolution and non-invasive 3D cross-sectional images, thus rendering it valuable for xthe diagnosis of diseases such as cataracts and glaucoma (15-18). In 1988, Phillips *et al.* (19), using

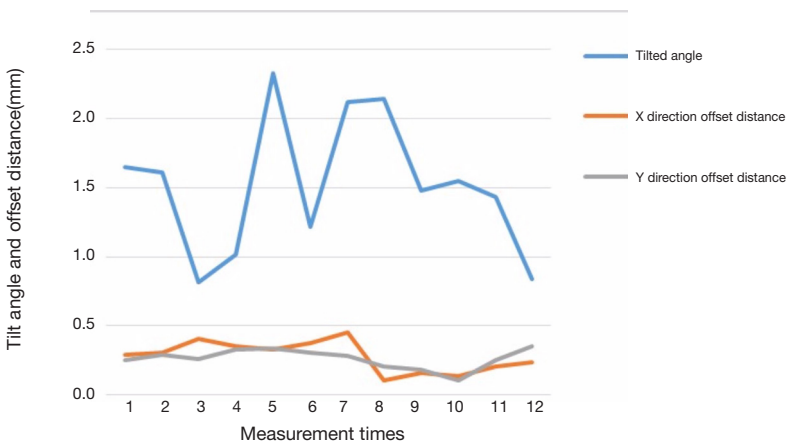

Figure 8 Data sheet for repetitive studies.

Table 2 Distance of IOL relative to the pupil and tilt angle in OCT images

Category	Mean ± SD (n=80)
X direction offset distance	0.29±0.22 mm
Y direction offset distance	0.33±0.24 mm
Eccentric distance	0.44±0.33 mm
Tilt angle*	1.65±1.00 degrees

*, indicates the scleral plane. IOL, intraocular len; OCT, optical coherence tomography.

Purkinje imaging system measured the tilt and decentration of IOL in the static eye. The results showed that the average tilt was 7.8 degrees and the average decentration was 0.7 mm. With the development of surgical technique and newly designed IOL presented on the market, the precise location of the IOL is crucial for better visual quality of patients. Even minute shift of IOL could induce refractive error and high order aberration. The traditional evaluation of the IOL position is based on slit-lamp images, which could not qualify, even detect, the minute dislocation of the IOL. Although the Purkinje method could qualify the small shift of IOL, it depends on reflected lights by many ocular compositions and complicated calculation, which is hard for clinician to understand and interpret. A reliable and objective method to quantify the IOL dislocation is indispensable for clinician, which might provide valuable information for IOL design and surgical strategy making.

OCT is a non-invasive, widely used and highly reliable 3D imaging method. In this study, we proposed a 3D-reconstruction method to calculate the tilt and decentration of IOL using a commercial OCT imaging system. It is different from the Purkinje or Scheimpflug imaging system and ultrasound biomicroscopy (UBM) (2,19,20). Compared with the previous Purkinje and UBM systems, our method is more convenient and accurate. The Scheimpflug systems has many limitations. For example, when lenses are very flat, it relies on the proper measurement of the anterior and posterior lens radius of curvature. The Scheimpflug system requires pupil widely dilated, which could not be achieved in some eye with IOL, especially for the IOL with obvious tilting. However, the majority of researchers have found that the clinically relevant tilt and decentration were limited, which is consistent with our results. This model took longer than the single-line scan model. Therefore, several potential factors in AS-OCT image capturing may affect the tilt and decentration values, such as the lack of an eye-tracking technique, the lower scan speed, the relatively longer capture time, the lack of a real-time capture technique for the eye plane image, and the cross-sectional image and fixation fluctuation of the patient.

In our study, we chose a spherical IOL for 3D reconstruction because the surface of the IOL is the most widely used, and the surface IOL is relatively convenient for performing 3D reconstruction. Of course, each patient's IOL is different. In this experiment, several sets of data were randomly selected for OCT images to ensure the accuracy of the experiment. Moreover, our method did not use equipment to realize the 3D reconstruction of IOL, which requires researchers to make subsequent calculations. The mathematical model we chose in the study was very accurate. We used the plane of the sclera as a reference surface to determine whether the IOL was tilted or eccentric. In the course of the experiment, there were still some issues relating to the middle of the IOL. In addition, we may need to use some other methods to analyze the location of the IOL for comparison. The OCT images used in our experiment were the postoperative OCT images of patients collected in recent years. We did not find the AS-OCT image database on IOL on the Internet, so our method could not be compared with other experimental results.

Acknowledgments

Funding: Funding was provided by the Beijing Municipal Administration of Hospitals' Youth Programme (QML20180202) and the National Natural Science Foundation of China (Grant U1713220).

Footnote

Reporting Checklist: The authors have completed the MDAR reporting checklist. Available at http://dx.doi.org/10.21037/atm-20-4706

Data Sharing Statement: Available at http://dx.doi.org/10.21037/atm-20-4706

Conflicts of Interest: All authors have completed the ICMJE uniform disclosure form (available at http://dx.doi.org/10.21037/atm-20-4706). The authors have no conflicts

of interest to declare.

Ethical Statement: The authors are accountable for all aspects of the work in ensuring that questions related to the accuracy or integrity of any part of the work are appropriately investigated and resolved. All procedures performed in this study involving human participants were in accordance with the Declaration of Helsinki (as revised in 2013). The study was approved by the Ethics Committee of the Beijing Tongren Hospital (TRECKY2018-066). Informed consent was taken from all the patients.

References

1. Kránitz K, Miháltz K, Sándor GL, et al. Intraocular lens tilt and decentration measured by Scheimpflug camera following manual or femtosecond laser-created continuous circular capsulotomy. J Refract Surg 2012;28:259-63.
2. Detry-Morel ML, Van Acker E, Pourjavan S, et al. Anterior segment imaging using optical coherence tomography and ultrasound biomicroscopy in secondary pigmentary glaucoma associated with in-the-bag intraocular lens. J Cataract Refract Surg 2006;32:1866-9.
3. de Castro A, Rosales P, Marcos S. Tilt and decentration of intraocular lenses in vivo from Purkinje and Scheimpflug imaging. Validation study. J Cataract Refract Surg 2007;33:418-29.
4. Mura JJ, Pavlin CJ, Condon GP, et al. Ultrasound biomicroscopic analysis of iris-sutured foldable posterior chamber intraocular lenses. Am J Ophthalmol 2010;149:245-52.e2.
5. Spadea L, Iozzo N. EBOV-RNA test with RT-PCR in ocular fluids of Ebola survivors can help to safely perform cataract surgery. Ann Transl Med 2018;6:S29.
6. Eppig T, Scholz K, Löffler A, et al. Effect of decentration and tilt on the image quality of aspheric intraocular lens designs in a model eye. J Cataract Refract Surg 2009;35:1091-100.
7. Baumeister M, Bühren J, Kohnen T. Tilt and decentration of spherical and aspheric intraocular lenses: effect on higher-order aberrations. J Cataract Refract Surg 2009;35:1006-12.
8. Oshika T, Sugita G, Miyata K, et al. Influence of tilt and decentration of scleral-sutured intraocular lens on ocular higher-order wavefront aberration. Br J Ophthalmol 2007;91:185-8.
9. Gillner M, Eppig T, Langenbucher A. Automatic intraocular lens segmentation and detection in optical coherence tomography images. Z Med Phys 2014;24:104-11.
10. Dai J, Li Y, He K, et al. R-fcn: Object detection via region-based fully convolutional networks. Advances in Neural Information Processing Systems 29 (NIPS 2016) 2016:379-87.
11. Lenc K, Vedaldi A. R-cnn minus R. arXiv:1506.06981, 2015.
12. Lin TY, Maire M, Belongie S, et al. Microsoft coco: Common objects in context. In: Fleet D, Pajdla T, Schiele B, et al., editors. Computer Vision – ECCV 2014. ECCV 2014. Lecture Notes in Computer Science, vol 8693. Springer, Cham.
13. Remington LA, Goodwin D. Clinical anatomy of the visual system E-Book. Elsevier Health Sciences, 2011.
14. Ren S, He K, Girshick R, et al. Faster r-cnn: Towards real-time object detection with region proposal networks. Advances in Neural Information Processing Systems 28 (NIPS 2015) 2015:91-9.
15. Werner L, Michelson J, Ollerton A, et al. Anterior segment optical coherence tomography in the assessment of postoperative intraocular lens optic changes. J Cataract Refract Surg 2012;38:1077-85.
16. Kanellopoulos AJ. Laboratory evaluation of selective in situ refractive cornea collagen shrinkage with continuous wave infrared laser combined with transepithelial collagen cross-linking: a novel refractive procedure. Clin Ophthalmol 2012;6:645-52.
17. Bianciotto C, Shields CL, Guzman JM, et al. Assessment of anterior segment tumors with ultrasound biomicroscopy versus anterior segment optical coherence tomography in 200 cases. Ophthalmology 2011;118:1297-302.
18. Kiddee W, Trope GE. Glaucoma tube imaging using anterior segment optical coherence tomography in patients with opaque cornea. J Glaucoma 2013;22:773-5.

19. Phillips P, Pérez-Emmanuelli J, Rosskothen HD, Koester CJ. Measurement of intraocular lens decentration and tilt in vivo. J Cataract Refract Surg 1988;14:129-35.
20. Girshick R. Fast r-cnn[C]//Proceedings of the IEEE international conference on computer vision. 2015:1440-8.

(English Language Editor: J. Gray)

Cite this article as: Xin C, Bian GB, Zhang H, Liu W, Dong Z. Optical coherence tomography-based deep learning algorithm for quantification of the location of the intraocular lens. Ann Transl Med 2020;8(14):872. doi: 10.21037/atm-20-4706

